Experimental study of quantum size effects in thin metal films by electron tunneling

R. C. Jaklevic and John Lambe
Scientific Research Staff, Ford Motor Company, Dearborn, Michigan 48121
(Received 19 May 1975)

Periodic structure in the electron tunneling spectra of Pb, Mg, Au, and Ag has been observed. Such spectra represent in fact a direct observation of size-dependent electronic states in thin metal films. Films with thicknesses from 100 to 1000 Å were studied and the effect on the electronic standing-wave energies was measured. The physical model for these effects and their observability involve the existence of so-called commensurate states. The spacing of the quantized energy levels provides a direct measurement of the electron group velocity while their location in energy determines the position of band edges and other critical energy states in the band structure of the metals. In some cases, the effective mass can also be determined. A qualitative theoretical picture is sufficient to understand all of the sailient features of the observations. A number of experiments including alloying, strain, and electric field modulation are also described.

I. INTRODUCTION

In previous publications,[1] the observations of quantized electron standing-wave states in thin films of Pb and Mg were reported. These experiments are described here in more detail. In addition, observations on Au and Ag are reported. These experiments involve metal-oxide-metal thin-film tunnel junctions in which the metal electrodes are vacuum deposited under optimum conditions for smoothness and crystal texture. Tunneling oxide layers are produced which will withstand several volts bias. The experimental results include the observation of standing-wave structure reflected in the conductance-versus-voltage curves taken at 4 and 77 °K together with a study of how the observed periodicity varies with film thickness and perturbations of strain, electric fields, overlays, alloying, and temperature. Critical band-structure parameters and their dependence on temperature and thickness are determined. These effects have been observed in spite of the inevitable lack of surface smoothness on a microscopic scale. It is shown that it is necessary to consider a film, which is made up of many small grains, as a composite crystal made up of "quantum boxes" which are of differing thicknesses but always an integral number of atomic layers. As a result, there are regions in the band structure where the box-quantized energy levels of the crystal grains will tend to align and therefore be observable. A simple theoretical picture will be described which adequately accounts for all of the observed effects.

II. THEORETICAL CONSIDERATIONS

A. Quantum box

In order to describe a thin metal film, it is useful to consider a deep potential well in which the thickness w is very small while the other two dimensions are very large. The electronic standing-wave states of this well are easily calculated by elementary quantum mechanics, and it is found that k, the component of momentum perpendicular to the film, is restricted to values

$$k = n(\pi/w), \quad n = 1, 2, 3, \ldots \quad . \tag{1}$$

The energy levels, measured from the bottom of the well, are $E = E_n + E(k_{\parallel})$, where $E(k_{\parallel})$ is the energy associated with motion parallel to the film surface and

$$E_n = (\hbar^2/2m)(n\pi/w)^2 \quad . \tag{2}$$

Adjacent levels are separated by an energy which is small compared with the well depth. The E_n values locate a set of states which are detected in tunneling measurements.

Considering the possibility of observing such a series of energy levels in a real metal film, a major problem arises from surface nonuniformities, i.e., roughness. Since the position of the energy levels is determined by w, careful control of this dimension would be necessary. A variation δw in thickness results in a shift of an energy level by

$$\delta E_n = -2(\delta w/w) E_n \quad , \tag{3}$$

while for large n, the spacing between levels is

$$\Delta E_n = (2/n) E_n \quad . \tag{4}$$

The condition for observability would be that

$$\tfrac{1}{2} \Delta E_n > \delta E_n \tag{5}$$

or

$$\delta w/w < 1/2n \quad . \tag{6}$$

For $n = 100$, this corresponds to a smoothness of 1%, corresponding to a single atomic layer, a very difficult requirement. This condition demands that the surface be smooth to within one electron wavelength, about 10 Å.

B. Crystalline quantum box

Fortunately, it is possible to relax this condition in the case of real metal films when account is taken of the properties of the crystalline quantum box. Although variations in thickness over the surface of the film are to be expected, these are not continuous but must correspond to an integral number of lattice spacings. Films are typically composed of an array of individual grains,[2] each grain oriented with the same crystal axis perpendicular to the substrate, with random orientation about this axis. The thickness will vary slightly from grain to grain and the possibility of some variation in thickness across a given grain cannot be ruled out. Each section of the film has a thickness $w = Nd$, where d is the lattice spacing and N is the number of atomic layers of the section. The film is an ensemble of sections with differing N values, and the energy levels of this composite are to be taken as a sum of all the quantum boxes of the film. It is assumed that the lateral dimensions of each section are sufficiently large and that the one-dimensional description of the quantum box is adequate.

Consideration of such a composite will show that even though the requirement that all levels with the same n must line up cannot be satisfied in practice, there still will exist certain states of a certain momentum, but with various n values, whose energy levels will coincide in spite of roughness. These are called commensurate states and are states whose electron wavelength is commensurate with the crystal lattice. A mathematical expression for this set of energy levels can be derived by the following model:

As before, the potential well is considered sufficiently deep so that the wave functions vanish at the walls. For each section of the film, the energy levels are determined by the condition of the electron wave vector given in Eq. (1), but with

$$w = Nd, \quad N = 1, 2, 3, \ldots$$

and hence

$$E_n(N) = (\hbar^2/2m)\,(n\pi/Nd)^2 \ . \tag{7}$$

Since the actual experiment deals with a large ensemble of sections of differing N, it is necessary to average over these by employing a distribution function $P(N)$ which determines the distribution of thickness of the various sections of the film. Each section of the film is assumed to be perfectly smooth. For the present experiments, a spread of $\pm 5\%$ about $N = 100$ might be considered typical. It will be assumed that $P(N)$ can be modeled by a Gaussian function,

$$P(N) = P_0\, e^{-\alpha(\bar{N}-N)^2} \ , \tag{8}$$

where $(\alpha)^{-1/2}$ is the experimentally determined width parameter of the distribution and $\bar{N}$ is the average atomic thickness of the film. Also, it is necessary to provide that the levels will not be perfectly sharp but will have a finite width $\hbar/\tau$ due to lifetime effects. Each level can be given a Lorentzian distribution

$$\rho(E - E_{n,N}) = \frac{2}{\pi}\,\frac{\tau/\hbar}{1 + (E - E_{n,N})^2\tau^2/\hbar^2} \ , \tag{9}$$

where τ, the lifetime of an individual state, is assumed independent of n and $\int_{-\infty}^{\infty} \rho\, dE = 1$. For each value of N, there will be a series of these states, and a distribution of states R for the entire ensemble of quantum boxes can be defined by

$$R(E) = \sum_N \sum_n \rho(E - E_{n,N})\, P(N) \ , \tag{10}$$

where $P(N)$ describes the roughness of the film as defined in Eq. (8). Quantitatively, this procedure is equivalent to superimposing a large number of energy ladders of nearly equal spacing. It will turn out that the quantized nature of the thickness of the crystalline boxes will select certain states in the band structure of the metal, called commensurate states, near which the individual ladders tend to come into registry with one another, and hence become observable. It is most instructive to study Eq. (10) for the case of a free-electron model in which attention is given to states whose wave vector in the reduced zone is given by

$$k = (S/Q)\,(\pi/d) \ , \tag{11}$$

where S/Q represents an irreducible rational number. It will turn out that the lower values of Q are the easiest to observe, but values up to 5 have been observed in some cases. The sketch in Fig. 1 shows a simple reduced-zone scheme with a few of the commensurate points labeled with a few S/Q values.

As remarked above, in the vicinity of one of these commensurate states, there will be a tendency for states of various film sections to line up and become observable. As is shown, $Q = 1$ corresponds to band-edge states while $Q = 2$ corresponds to the states halfway through the zone. Likewise, $Q = 3$ states are one-third and two-thirds of the way through the zone, etc. Real band-structure effects will modify this picture, especially near a band edge, but this is not fundamental to the present discussion. A useful physical insight into the significance of commensurate states can be gotten by inspection of Fig. 2, where an example is shown of the real part of the electron standing-wave solution for a $Q = 1$ or $Q = 2$ state. Clearly, the $Q = 1$ state can always satisfy the boundary condition regardless of N, thus ensuring that there is always a state at this energy regardless of the thickness

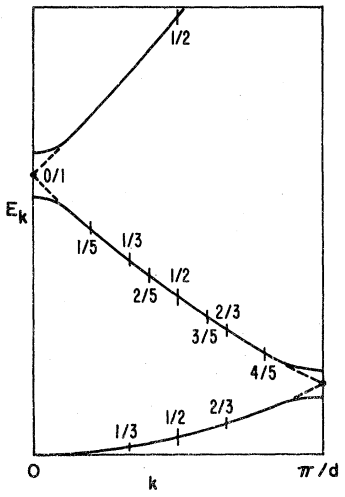

FIG. 1. Sketch of energy E vs momentum k for one direction in a simple metal, where a few commensurate points are indicated by their S/Q values. These states occur at momenta $(S/Q)(\pi/d)$. The band-edge momenta at 0 and π/d correspond to 0/1 and 1/1 points, respectively. Not all of the points will be accessible to experiment owing to voltage limitations on the tunneling oxide and the decrease in intensity with increasing Q.

of the crystal. Similarly the $Q=2$ state always satisfies the boundary condition when N is even. So, at the point $k=\frac{1}{2}(\pi/d)$, all quantum boxes of even N will have a state with this momentum, while all boxes of odd N will have a pair of states of either side of the halfway point, i.e., will interleave the even states. In an ensemble of crystalline quantum boxes, the commensurate state $E(\frac{1}{2}(\pi/d))$ will be fixed in energy. Simple analysis also shows that states near this level tend to line up with one another when a composite tunneling spectrum is obtained containing a range of grain thicknesses. The analysis will show that when levels with higher Q values are considered, nearby states will crowd in more and more and resolution will be lost.

In order to facilitate the analysis, the density of states for an ensemble of quantum boxes is calculated in the region of E vs k near a given commensurate state and, over that region, the curve can be approximated by a straight line or a parabola. For example, near a band edge, $Q=1$, and the energy-level spacing for a box of thickness Nd will be

$$\Delta E=(\hbar^2/2m^*)n'(\pi/Nd), \quad n'=1, 2, 3, \ldots, \quad (12)$$

where the index n' determines the spacing starting at the band edge and m^* is the effective mass near the edge. On the other hand, away from band edges, the group velocity v_g will be nearly constant over small energy intervals and

$$\Delta E=\hbar v_g(\pi/Nd)\ . \quad (13)$$

For this case $\Delta E=(dE/dk)\Delta k$, where $v_g=(1/\hbar)\times(dE/dk)$ and $\Delta k=\pi/w$. Recall that for $Q=2$, the observed intervals for an ensemble will be $\Delta(\text{eV})=\Delta E/2$ owing to interleaving of odd and even layered boxes.

The sum, Eq. (10), must be computed for an ensemble of N values which occur in typical films. As shown in Fig. 3, this sum can be illustrated for a film which is assumed to contain an equal number of each thickness, with N ranging from 95 to 105, i.e., a simple rectangular distribution function instead of a Gaussian. For this state, $S/Q=\frac{1}{2}$ and the energy levels for odd N just interleave those for energy N. The sum shows resolved levels around this $Q=2$ point with a splitting which is one-half the splitting of the odd or even N segments. Note that, since all of the segments are approximately the same thickness, within 5%, it is possible to speak of a characteristic splitting of the film. The levels will be experimentally resolved in the vicinity of the $Q=2$ point with a splitting of one-half the characteristic level separation. At a $Q=1$ point the actual level splitting would be observed, and in general in the vicinity of a commensurate level $1/Q$ times the actual splitting is observed.

A useful approximate analytic expression for Eq. (10) can be obtained for the simple case where v_g is considered constant. The distribution for a given

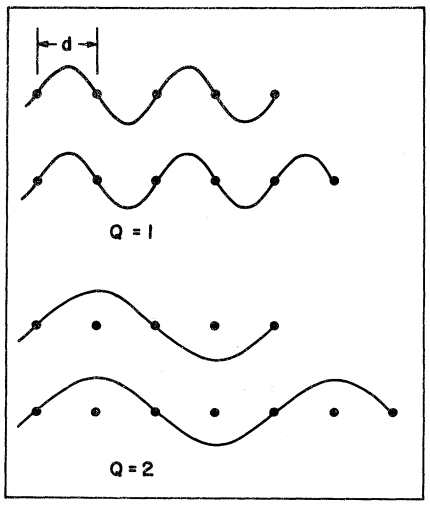

FIG. 2. Sketch of the electron standing-wave functions at the surface of a metal showing the relationship of the phase and wavelength to the atomic lattice of the metal. For electrons with momenta near a $Q=1$ point, $\lambda=2d$, and the addition of another atomic layer results in the same energy state. Likewise, for a $Q=2$ state, $\lambda=4d$, and the addition of two atom layers yields the same energy state. This is the basic physical mechanism for the tendency for groups of energy states to align near a commensurate state.

N can be expanded in terms of a Fourier series which can then be summed over N. For large N and reasonably narrow distribution in N the result is

$$R(E)=\bar{N}\frac{Q}{\beta}+\frac{1}{2}\bar{N}\frac{Q}{\beta}\exp\left(-\pi\frac{\hbar}{\tau}\bar{N}\frac{Q}{\beta}\right)\cos\left\{2\pi\left[E-E\left(\frac{S}{Q}\right)\right]\bar{N}\frac{Q}{\beta}\right\}\exp\left\{-\frac{\pi^2}{\alpha}\left[E-E\left(\frac{S}{Q}\right)\right]^2\left(\frac{Q}{\beta}\right)^2\right\}, \tag{14}$$

where $\beta/\bar{N}\equiv\hbar v_g\pi/d$ is the average level spacing. Only the first two terms of the series are retained since higher terms are not observed in practice. This formula displays a number of essential points of importance for the observation of standing-wave states: (a) The thickness distribution of quantum boxes determines the envelope function of the spectrum; (b) the lifetime affects the amplitude of the distribution but not the period; (c) large splittings, which allow for good observability, result when v_g is large; (d) the Q-number dependence of the period predicts small splittings for large Q, thus making observability more difficult; large Q also affects the amplitude of the oscillations adversely; and (e) the states near $E(S/Q)$ are least sensitive to thickness variations.

C. Electron tunneling as a probe of standing-wave states

It has been shown that a set of standing-wave states in a real metal will cause an oscillatory term in the density of states. The observation of these states by electron tunneling can be understood by means of a simple model. According to this point of view, the bulk of the tunneling current is made up of electrons with momentum approximately normal to the barrier. Specular tunneling is also assumed so that, with conservation of $k_{\parallel}$, only states with small $k_{\parallel}$ will be involved. This is a simplistic model which in the end must be justified by the experiment.

According to the model, the electron current flowing into an unoccupied standing-wave state would have the form shown in Fig. 4. where a finite tunneling barrier is assumed. The current initially has the form of a slanted step which eventually dies off exponentially with voltage. Thus the conductance is peaked at V_n and then dies off. The sharpness of the peak depends on the details of the barrier. If this peak is sharp compared to other broadening mechanisms, each peak in conductance can be identified with a standing-wave state. The distribution of states already discussed will then be mapped out by the conductance. When lifetime-broadening effects are included the position of the level will not occur exactly at peaks in conductance. In fact, a careful analysis of this problem has been carried out and, for the experimental condition encountered in these experiments, it is more accurate to locate the levels at peaks in the second derivative. This has been presented in another publication.[3] Recently, Wolf[4] has raised the point that lifetime effects may increase the tendency toward peaking in conductance. Such effects would need to be considered

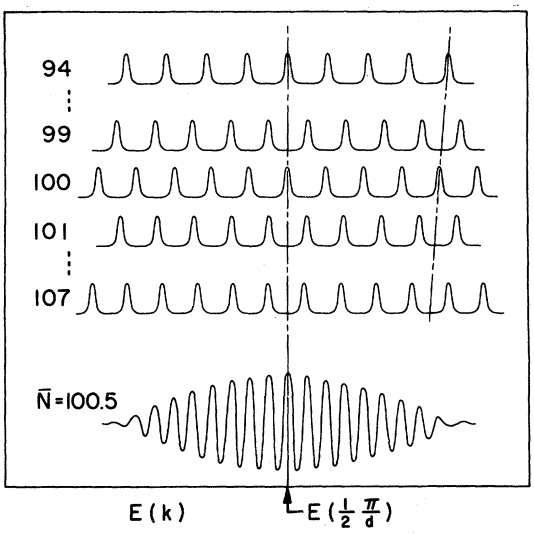

FIG. 3. Sketch of a simple model calculation of the expected spectrum for momenta near $k=\frac{1}{2}(\pi/d)$ and for a distribution of grain sizes with $\bar{N}=100.5$. Each thickness is given equal weight and the individual states have a Lorentzian shape. The tendency of these states to line up near $\frac{1}{2}(\pi/d)$ and then lose resolution away from this point is evident.

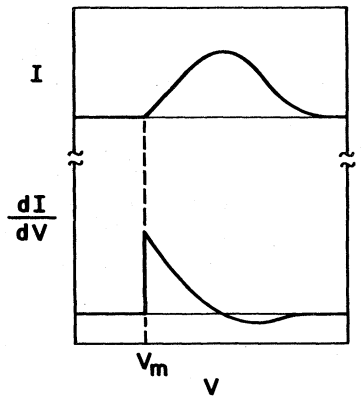

FIG. 4. Sketch showing the current I and conductance $G=dI/dV$ vs V for tunneling into a single standing-wave level. In voltage, this state is located at V_n with respect to the Fermi level. The sharp peak in G occurs at V_n and the current tails off to zero at higher voltages owing to barrier effects. Lifetime broadening is not included.

in a more rigorous theory of tunneling and standing-wave states.

D. Lifetime of states

It is clear that the lifetime τ of the individual states must not be so small as to reduce the pattern amplitude given by Eq. (14) to unobservable size through smearing of the levels. It requires that the films must be sufficiently thin that energy-level spacing will be greater than the lifetime broadening. An additional limitation associated with the surfaces will occur owing to the finite reflectivity of the walls of the quantum box and the lack of specularity of the reflection. Thus it is useful to discuss the lifetime in terms of the bulk lifetime τ_b and the surface-related lifetime τ_s,

$$1/\tau = 1/\tau_b + 1/\tau_s \ . \tag{15}$$

The surface term can be approximated by

$$1/\tau_s = [(1-r)/r]\, v_g/w \ , \tag{16}$$

where r is the specular reflectivity, i.e., the probability that an electron will reflect specularly from the walls of the box, and v_g/w is the number of reflections per second. The important point of Eq. (16) is that τ_s gets smaller as the box is made thinner, an important point for the feasibility of these measurements. On the other hand, τ_b will set an upper limit on the thickness, so that a limited thickness range will exist for observability of these states. In these experiments, there has been no clear-cut effects attributable to τ_s since other problems related to thin-film fabrication limit film thickness to over 100 Å.

The bulk lifetime τ_b is widely discussed in the literature. For the present case, it must be noted that the observed states correspond to electrons well removed in energy from the Fermi level. These "hot" electrons can have lifetimes considerably shorter than those near the Fermi level. The decay process for this case has been discussed by Quinn and Thomas.[5] The primary decay process is the electron-electron interaction; for the energies of interest, there will be no plasmon creation, so that individual particle collisions will dominate. For an electron excited to 1 or 2 eV above the Fermi level, a lifetime of about 10^{-13} sec is expected, giving an energy width of about 25 meV. This assumes a group velocity of 10^8 cm/sec, with a corresponding mean free path of 1000 Å. These estimates give some idea of what lifetime broadening to expect and how large a spacing can be observed.

E. Effects of alloying, electrical modulation, and strain

The picture so far describes the observable set of states located at certain energies with respect to the Fermi level. This section discusses methods whereby these levels can be shifted, thus verifying some important details of the model and giving further insight into the quantum-box problem in metal films. An obvious way to shift the observed standing waves with respect to the Fermi level is to shift the Fermi level itself, by doping the metal with foreign atoms and thereby changing the electron/atom ratio. The simple rigid-band model of alloy effects predicts that for the case of Pb, which has 4 electrons/atom, the addition of Bi, with 5 electrons/atom, would raise the Fermi level. A resulting shift of the observed standing-wave states will thus directly test this simple picture. This is the so-called rigid-band model of alloy effects in its simplest form.

A second method for shifting the energy levels is via the electric field at the surface of the metals. The technique for this is shown schematically in Fig. 5. An auxiliary field electrode is provided whereby a variable potential can be applied between it and the outer surface of the metal film. The intervening insulator is sufficiently thick so that no current can flow, but thin enough so that fields of the order of 10^6 V/cm can be applied to the surface of the quantum box. This electric field is responsible for the shift in the energy levels as observed with the tunneling current. The mechanism by which this shift occurs is essentially the result of the perturbation of the electron energy levels in the

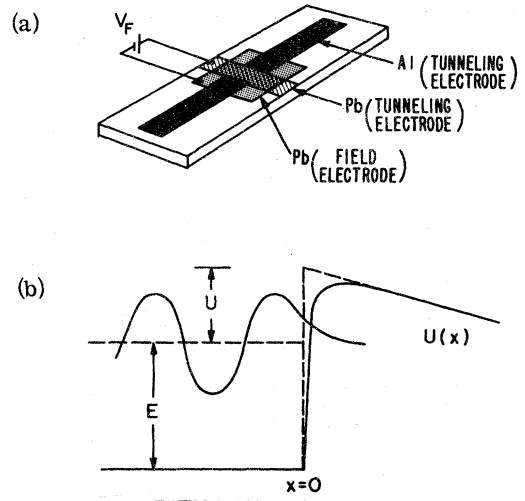

FIG. 5. Schematic drawing of the electric field effect modulation technique. In (a) the tunnel diode is shown as crossed Al and Pb strips. The third (square) Pb electrode is separated from the middle Pb strip by a 1000-Å SiO insulating film. The potential energy $U(x)$ of an electron near the surface ($x=0$) of the Pb tunneling electrode is shown in (b), where the contributions due to the image potential and applied field (linear term) are both included. The electron standing wave is also indicated, with the part which overlaps the region of the applied field ($x=0$) being responsible for the electric field energy shift.

film by overlap of their wave function with the applied electric field. This occurs in those regions just outside the metal where the electron wave extends into the image-potential region and decays exponentially inside the barrier. An accurate theory of this effect based on a complete quantum-mechanical model has not been done. However, an estimate of the size of the effect may be made by treating the electric field perturbation as effectively changing the dimensions of the quantum box by the amount

$$\Delta w = \tfrac{1}{16} C^2 e^3 F / U_0^3 , \tag{17}$$

where U_0 is the electron energy referred to the barrier top (Fig. 5), F is the applied electric field, $C = e/4\pi\epsilon_0\kappa$, and it is assumed that the potential energy of the electron just outside the metal is given by $U(x) = -eFx - Ce/4x$. For typical values of $U_0 \simeq 3$ eV, $\kappa = 4$, and $F = 3\times 10^6$ V/cm, a shift of several hundred μV is expected.

A third method of level modulation is strain, which we have described in a previous paper.[6] This technique is useful because it is able to separate standing-wave or band-structure effects from background effects and is typically ten times bigger than the electric field modulation. Background effects would include molecular excitation contributions and barrier effects. Thus a strain-derivative method can be used to advantage. The film thickness, and therefore the size of the box, can be effectively changed by 0.1% by simply bending the substrate. On a free-electron model, shifts of band levels can be estimated by $\delta E/E \simeq -2\delta w/w$ so that a shift $\delta E \sim 20$ meV can be achieved, well within experimental detectability. These measurements can also be used to aid in understanding observed shifts due to thermal expansion effects. Both the magnitude and the sign of the strain shift are of use in identfying unknown tunneling structure. In the case of a film attached to a ceramic or glass substrate, the major expansion effects will be the thickness of the metal film, which can be changed by almost 1% between 4 °K and room temperature. Thus the thermal expansion produces non-negligible effects on the levels of a quantum box.

F. Effect of temperature and thickness on band states

The observation of standing-wave states by tunneling provides a measurement of certain critical band energy levels, the commensurate levels. The values of these energies can be expected to depend on temperature. A weak dependence on thickness may also be anticipated owing to surface effects. The $k = \frac{1}{2}(\pi/d)$ state of Pb has been studied most extensively in this regard. In particular, the level shifts to lower energies with increasing temperature and shifts to slightly higher energies with decreasing thickness. In the former case, the shift can be understood in terms of the change in lattice constant of the metal with temperature. The energy shift can then be related to this change by the strain-dependence measurements. The latter effect is understood by noting that a certain fraction of the total wave function of the electron extends outside the metal through barrier-penetration effects. This amounts to a surface contribution to the energy of the state. For thinner films, this term increases in relative importance. An estimate of its size can be made by referring to the exact solutions of the potential-well problem with finite depth.[7]

III. EXPERIMENTAL METHODS

The detailed methods of producing the tunnel junction for these experiments have been described in detail elsewhere[8] and will not be repeated here. Rather, those points of significant departure from previous methods will be emphasized. Briefly, the techniques were modified to produce better insulating tunneling layers on aluminum so that higher-voltage tunneling diodes could be produced. Attention was also given to producing smooth films of the proper thickness with maximum purity.

The fabrication of the tunnel diodes starts with the vacuum deposition of a thin Al strip about 2 mm wide on a glazed ceramic substrate $\frac{1}{2}\times 1\frac{1}{2}$ in. The thickness of the Al for many of these has been limited to about 400 Å after it was found that the diodes were more stable at several volts bias, probably because the Al-base films are smoother in this thickness range than for the 1000 Å used previously. This was followed by a gas anodization of the aluminum film to produce the insulating tunneling layer. The anodization proceeds for 45–75 min under a pressure of 0.1 Torr of O_2 with a discarge voltage of 500 V and current of 10 mA. When the crossing overlay films are Pb, pure O_2 is used, while for overlays of Au, Ag, and Mg, an initial charge of 0.05 Torr of water vapor is admitted to the vacuum chamber and then the O_2 flow is initiated. This H_2O treatment produces diodes with good stable characteristics which are better able to withstand the necessary voltages. The evaporation of the top metal electrode was done by evaporation of 99.999%-pure or better material from resistance-heated boats at a pressure of about 10^{-7} Torr. The rates varied somewhat, but were of the order of several hundred Å/min as monitored with a quartz-crystal microbalance. The substrates were kept cold during this evaporation by mechanically fastening them to a liquid-N_2-cooled copper block. For Pb and Mg, temperatures of about 150 °K were found optimum, while for Au and Ag the lowest temperature obtainable, about 90 °K, was found to be best. This step gives films which are smooth and which anneal upon warming to room temperature. Thus smooth, tex-

tured films are produced. The texture, or degree of alignment of the film grains, was verified by x-ray diffraction. For Pb, Ag, and Au, a [111] texture is observed, while for Mg, a [0001] texture is observed. The diodes have resistances of about 1–10 Ω or more, which will gradually increase to several hundred ohms in a few days, a resistance more optimum for study.

For the electric field modulation, a third field electrode was introduced by evaporation of a silicon monoxide film 1000 Å thick over the tunnel diode, and then a third electrode of Pb was deposited to complete the triode structure, as shown in Fig. 5. Several tens of volts could be applied across this insulator, corresponding to fields of several million V/cm without any appreciable current flow.

The measurements were carried out between 4 and 300 °K. For some cases it is advantageous to measure at 4 °K, since the size of the effects is greater. Although the smearing of the electron distribution near the Fermi level sets an upper limit to the temperatures, the structure of interest in these experiments is sufficiently broad that 77 °K is usually enough. Large effects, such as those due to band edges, can be observed at 77 °K with little difficulty.

The strain-effect measurements were performed in a manner described before.[6] The substrates were bent by application of a weighted rod to the slide supported at its ends. The applied strain was along the length of the film, and was about 0.1% and varied only slightly from substrate to substrate. The actual resulting strain along the tunneling direction, perpendicular to the substrate, is of opposite sign and of the same order of magnitude as the applied strain.

The doping was done by mixing a small amount of Bi with the Pb charge in the evaporation boat and allowing them to melt together before evaporation temperatures were reached. Both metals have similar vapor pressures; therefore preferential evaporation effects are not considered to be a problem.

The electrical properties of the tunnel diodes were measured by means of a differentiation technique using ac harmonic detection. The conductance $G = dI/dV$, the second derivative d^2I/dV^2, or the third derivative d^2G/dV^2 of current could be measured versus the applied voltage V. A circuit described previously[8] was used, with the exception that the input transformer for measurement of the ac voltage across the junction was replaced by a series-resonant impedance-matching circuit. The latter is adjustable and more convenient to use. A ramp from a digital signal averager[9] provides the dc voltage bias applied to the tunnel diode, and the resulting tunneling spectra are stored in the 1024-channel digital memory. A 2-sec sweep time is typical. Subsequent sweeps can be added to the stored spectra to produce an averaged spectrum. The stored spectra can be examined by means of an oscilloscope readout. The use of a digital signal averager allows for easy handling of the field effect or strain-modulated tunneling data. When one of these perturbation methods is under study, an initial unperturbed spectrum can be stored in the memory. Subsequently, the field or strain is applied and the perturbed spectrum is subtracted from the first one, with the result that only those portions of the spectra sensitive to field or strain effects remain. Thus field or strain modulation spectra can be obtained with ease. Permanent data storage is accomplished by recording the spectra on paper with an x-y recorder or via photographic techniques from the oscilloscope readout.

IV. EXPERIMENTAL RESULTS AND DISCUSSION

A. Lead

Low-temperature spectra. The tunnel conductance vs voltage at 4 °K for an Al-(Al oxide)-Pb diode is shown in Fig. 6. The curve shows prominent oscillatory structure superimposed on a gradually increasing background. The Pb is positive for this polarity, so energy states of interest here are in the [111] direction and lie above the Fermi level of Pb. Note that the oscillations are centered at about 0.85 V. For a Pb thickness of 167 Å a period of 0.120 V is measured. If the thickness of the Pb is changed, the period of the oscillations changes, but the center of the spectrum remains near 0.85 V. Figure 7 shows a d^2I/dV^2 vs voltage curve for a similar diode with the Pb 234 Å thick. The oscillations resemble a set of interference

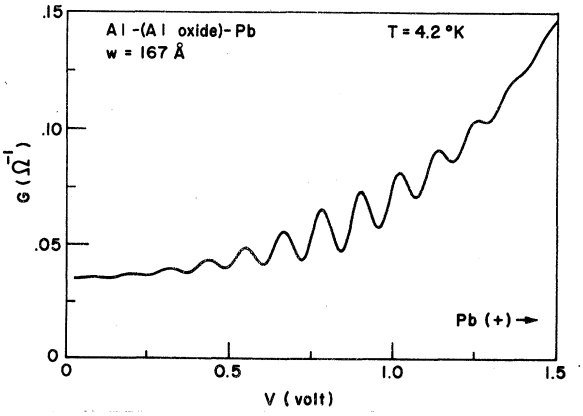

FIG. 6. Experimental plot of conductance $G = dI/dV$ vs voltage for an Al-(Al-oxide)-Pb tunnel junction at 4 °K for $w = 167$ Å. The Pb states from 0 to 1.5 V above the Fermi energy are scanned. The observed periodicity is due to a series of discrete electron standing-wave states above the Fermi level of Pb.

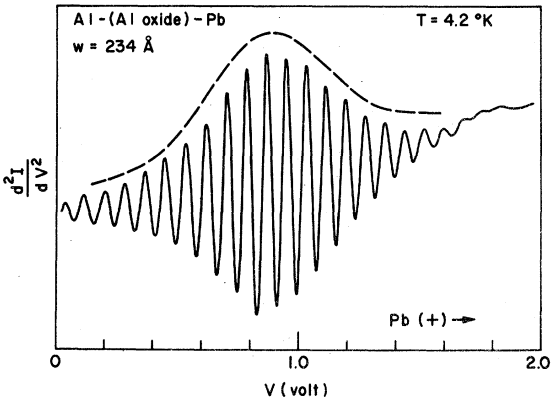

FIG. 7. Experimental plot of d^2I/dV^2 vs voltage for Pb covering the range from 0 to 2 V. The pattern exhibits a nearly Gaussian envelope shape and, from this data, an atomic film thickness distribution of 87 ± 7 atom layers is deduced from Eq. (14). The Gaussian envelope is plotted with a slight displacement upward from the data plot.

fringes centered at 0.85 V. The dependence of the period of these oscillations on the measured thickness is shown in Fig. 8, where the period varies as $1/w$, in agreement with the simple theoretical model. The group velocity obtained for Pb from this plot, assuming $Q=2$, is 1.93×10^8 cm/sec. A comparison of these numbers with those obtained from the calculated band structure of Pb in the [111] direction[10] is included in Table I, and a close agreement is found.

It is interesting to see how the fringe pattern changes with small changes in Pb thickness. This

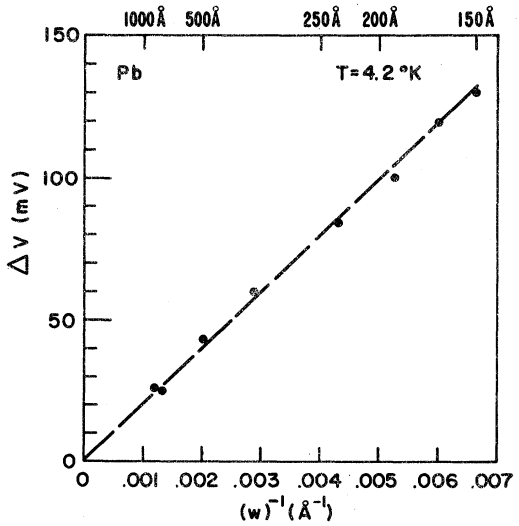

FIG. 8. Plot of observed periods of tunneling spectra vs $1/w$ for Pb for the $Q=2$ state. This plot is more extensive than previously reported, extending to 150 Å. The straight line corresponds to a group velocity of 1.93×10^8 cm/sec.

TABLE I. Comparison of experimentally determined band parameters for Pb at 4.2 °K along the Γ–L direction with values deduced from the theoretical band structure of Anderson and Gold. A positive sign means the state is above the Fermi level. Group velocities are determined at the corresponding commensurate state.

	Theory	Experiment
$E(\frac{1}{2}(\pi/d))$ (eV)	+0.75	+0.85 ± 0.05
v_g (cm/sec)	$\sim1.9\times10^8$	1.93×10^8
$E(\frac{2}{5}(\pi/d))$ (eV)	−0.61	−0.6 ± 0.1
v_g (cm/sec)	$\sim1.8\times10^8$	1.8×10^8
$E(\frac{1}{3}(\pi/d))$ (eV)	−1.42	−1.35 ± 0.01
v_g (cm/sec)	$\sim1.8\times10^8$	1.7×10^8

is done in Fig. 9, where two patterns are obtained from different diodes with slightly different Pb thicknesses. If attention is focused on two peaks located above and below the central peak, it is noted that, for the slightly thinner film, the peaks are further away from the stationary central peak. The difference in thickness of these films can be calculated from this to be 17 Å. This observation is a clear indication that the center of the spectrum is a $Q=2$ point of the [111] direction of Pb, as was

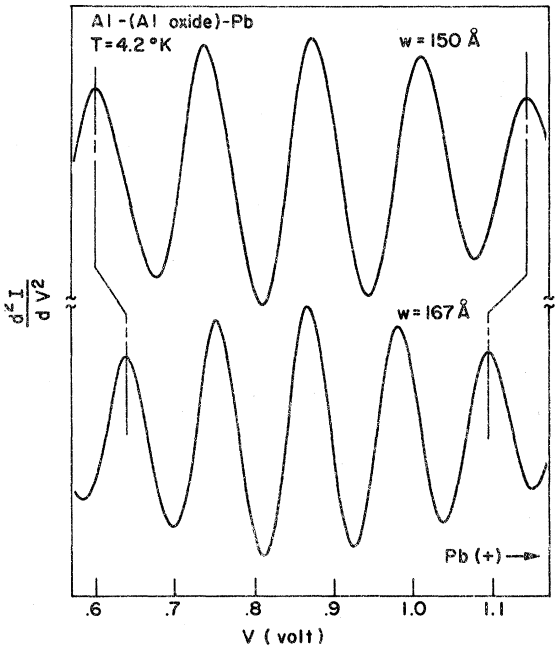

FIG. 9. Experimental plot of tunneling spectra showing d^2I/dV^2 vs voltage, showing the standing-wave pattern for two slightly different Pb thicknesses, 150 and 167 Å. The effect of the 17-Å difference on the periodicity is indicated by the connecting lines which also illustrate the lack of shift of the commensurate state with thickness.

noted before. This peak is stationary and the other observable quantized levels move with respect to it. An examination of a number of such plots indicates that the peak in d^2I/dV^2 is the best indicator of the position of the commensurate energy level, as was suggested before.

Figure 10 shows how d^2I/dV^2 behaves for two very different thicknesses. The observed amplitude of the conductance oscillations is largest for the 260 Å film and becomes smaller for the thicker film. This observation illustrates the effect of lifetime due to bulk scattering. Clearly τ_b will limit the observations to thicknesses below a certain maximum (about 1000 Å).

The observed structure centered at 0.85 V is contained in an envelope determined by the distribution of grain size, Eq. (4). Included in Fig. 7 is a Gaussian function plotted for reference using Eq. (14), where the width $\alpha^{-1/2}$ of the distribution is inferred to be 6 atom layers and $\bar{N} = 87$. This corresponds to a smoothness of ± 7% for this film. This width was fairly reproducible for a given thickness but could not be varied experimentally. On occasion, especially for the thicker films, much less symmetric envelopes were observed, as can be seen in Fig. 10.

One result of making the films thinner is that the center of the spectrum tends to shift slightly to higher voltages. For example, a 250-Å film had a commensurate energy smaller by 10 meV than a 150-Å film. This behavior is expected for a quantum box with finite potential walls, since the penetration of the wave function into the barrier becomes a relatively greater contribution to the energy as the film is made thinner, i.e., the underlying band structure of the metal becomes thickness dependent. An estimate was made of the expected size of such an effect by comparing the calculated energy of the $k = \frac{3}{2}(\pi/d)$ extended zone states for two quantum boxes of thicknesses 300 and 100 Å for a film with a barrier height of 11.3 eV and $d = 3$ Å. The exact theory[7] for a particle in a box was used and it was found that the energy of this state was 80 mV higher for the thinner film compared to the thicker one. The agreement with experiment is not quantitative, but does indicate that such factors will adversely affect the precision with which the commensurate states can be located.

All of the data discussed so far refer to the $Q = 2$ standing-wave states, for k values halfway across the second zone of Pb in the [111] direction. On occasion in the very best films, other sets of commensurate states were observed, corresponding to $S/Q = \frac{2}{5}$, and showed a splitting of 0.05 eV centered at about 0.6 V below the Fermi level. This same film showed a splitting of 0.129 eV at the $Q = 2$ midband point, and the splittings are in the ratio of nearly 5:2, as expected. Since v_g is changing slowly with energy, the ratio is not precise. The $S/Q = \frac{1}{3}$ state was also observed, with splittings of 0.08 eV, which is nearly two-thirds of the midband splitting, as expected. Of course, the amplitude of these states was considerably smaller than the $Q = 2$ state, as Eq. (14) suggests.

In summary, Fig. 11 shows a plot of the energy vs k for the [111] direction of Pb in which the rele-

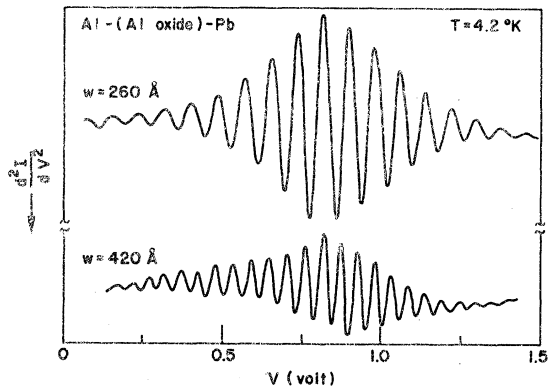

FIG. 10. Experimental plots of d^2I/dV^2 vs voltage for 260- and 420-Å Pb films. The amplitude of the pattern decreases with increasing thickness and the envelope tends to asymmetric shapes.

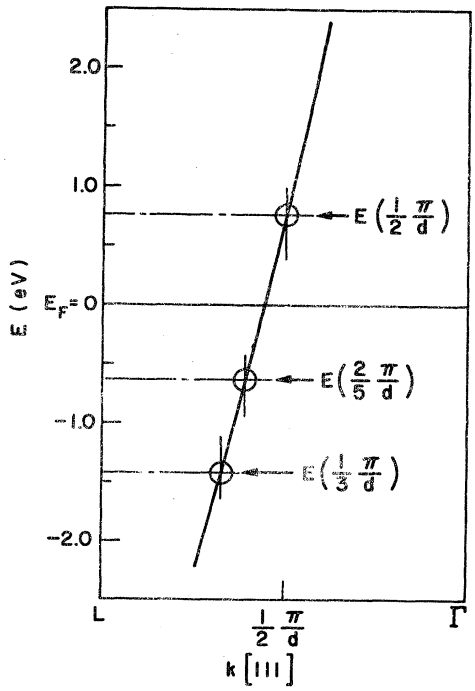

FIG. 11. Plot of the relevant part of energy vs momentum for the [111] direction of Pb from Ref. 9 showing the position of three observed commensurate states, $S/Q = \frac{1}{2}$, $\frac{1}{3}$, and $\frac{2}{5}$. The relevant energy and group velocities are listed in Table I.

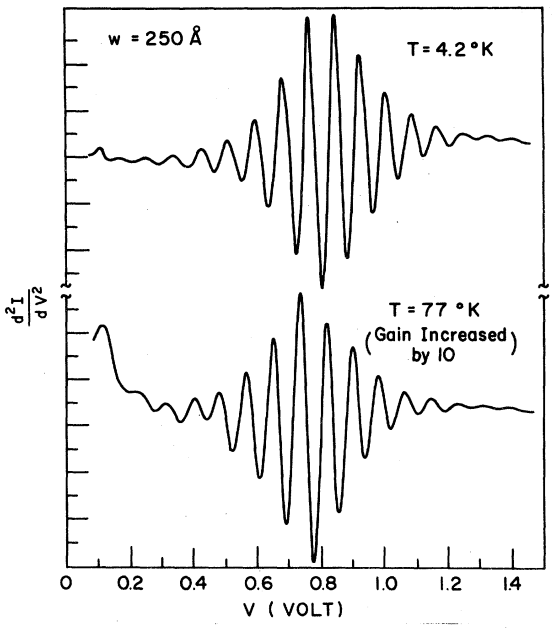

FIG. 12. Experimental plot of d^2I/dV^2 vs voltage showing the standing-wave pattern for 4 and 77 °K. There is a decrease in intensity and a slight downward shift of the pattern with increasing temperature.

vant states are indicated. Values of group velocity and commensurate state energies obtained for these experiments are listed in Table I and are compared with the theoretical[10] values.

Thermal effects. All of the above data on Pb were taken at 4 °K. It is expected that the temperature has a significant effect on standing-wave spectra and a number of observations have been made. Two d^2I/dV^2 spectra are shown in Fig. 12 comparing 4 with 77 °K behavior. There is a small shift in the center of the spectrum, and the amplitude of the structure is reduce considerably. The shift was measured from 4 to 200 °K, and the results plotted in Fig. 13. The center $Q=2$ states and the nearby levels move to lower voltages, i.e., moving closer to the Fermi level. This is simply attributed to the thermal expansion of the Pb film, since the lattice parameter d is increasing with temperature, and therefore the electron momentum $\frac{1}{2}(\pi/d)$ of the $Q=2$ state will decrease. Since the dependence of this energy level on strain has already been measured to be about 16 eV per unit strain for the [111] direction, [6] the expected shift can be computed from the thermal expansion data for Pb. [11] It is also necessary to take account of the effect of the ceramic (glazed alumina) substrate. This is most simply done by noting that the temperature coefficient of expansion of the ceramic is much smaller than the Pb in this temperature range, and so, for the purposes of this calculation, can be neglected. The effect of the substrate therefore is to cause a biaxial stress of the Pb film, resulting in a strain along the [111] direction in addition to the free change due to thermal expansion. This calculation was done for Pb and the predicted shifts are also plotted in Fig. 13. The agreement is surprisingly good for this simple picture. Over this temperature range one is observing changes in the lattice parameter of ~1% with electrons whose free-electron wavelength is about 1 Å.

The change in amplitude with temperature corresponds to a decrease by a factor of 20 in going from 4 to 77 °K for the best films. The change is less for films with correspondingly weaker structure at 4 °K. These facts make it difficult to interpret this amplitude change in detail, since it is clear that more than simple Fermi-level temperature broadening is involved. The reason for such a large effect is not understood. The states involved are about 1 eV above the Fermi level, and therefore their bulk lifetime should not be temperature dependent, based on the usual considerations involving electron-electron interaction. It is possible that surface scattering changes drastically, or perhaps a combination of kT broadening and some dependence of lifetime on temperature would be sufficient to explain this effect.

Observation of boundaries. One of the most direct experimental tests of the quantum-box ideas is alteration of the boundary. For these experiments the outer surface of the film is accessible and overlay materials can be added. A direct test is a comparison between spectra obtained from an untreated Pb film and a comparison film covered with a thin 25-Å Ag overlay. The structure is much weaker in the latter case and the splitting between

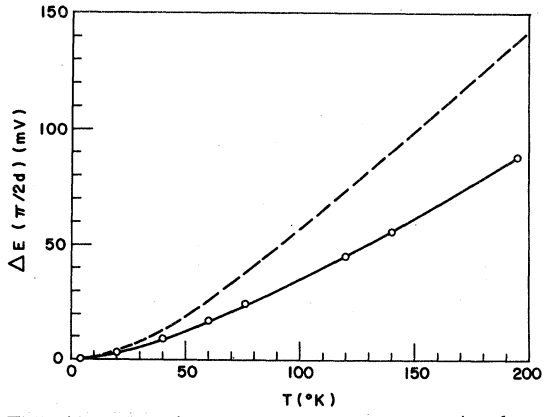

FIG. 13. Plot of observed shift ΔE of the $S/Q=\frac{1}{2}$ state in Pb vs temperature for $w=167$ Å. The increase can be accounted for in terms of the expansion of the Pb lattice with temperature. The dashed curve represents the expected change of the level with temperature, taking into account the effect of the substrate.

the levels decreased slightly. When the overlayer of Ag was made thick (500 Å), the structure was not observed. Clearly, with the presence of the overlay, the electrons in the Pb film do not have a high reflection coefficient so that the standing waves extend into the overlay. If, however, the outer Pb surface is first oxidized by exposure to oxygen before the overlay is applied, there is no overlay effect. The thin oxide decouples the electrons in the quantum box from the Ag overlay.

Pb alloys. As described already, the substitution of Bi atoms for Pb atoms should have the effect of raising the Fermi level. This was done by evaporating dilute alloys of Bi in Pb. In the observed spectra of these films the standing-wave spectrum near the $Q=2$ state was displaced to lower voltages by 75 mV. For this case 5 at.% Bi was added to the initial alloy. The final composition was not measured. The direction of the shift is just what one would expect if one "fills up" the Fermi sea.

Strain. As described before,[6] the strain-modulated standing-wave tunneling spectrum of Pb can be measured by the application of strain along the [111] direction. Briefly, the sign and magnitude of the +10-mV shift in the standing-wave states in response to a 0.06% strain is in excellent agreement with the estimate based on free-electron theory. For convenience, the experiments were carried out at 77 °K. The surface of the substrate was bent convex, so that a negative strain resulted in the [111] direction and the shift was to larger voltages. Also, it was observed that the spectrum was free of molecular vibration structure and the background effects due to the voltage dependence of the barrier.

Electric field modulation. As described above, a third field electrode was added to test the effect of an applied electric field on the standing-wave spectra. An electric field difference spectrum was taken in which the dc field of 3×10^6 V/cm was applied to the third Pb film (Fig. 5) was a 30-V dry cell. The zero-field spectrum was then subtracted to obtain the result. The standing-wave structure was observed to shift upward by 0.7 mV when the gate electrode was negative with respect to the Pb film and downward when the gate was positive. The sign of the effect is in agreement with expectations. Also, the size of the shift is in reasonable agreement with the 0.3-mV estimate using Eq. (17). Since the measured shift is consistently higher than predicted, it is possible that nonuniformities in the SiO layer could cause the local field at the Pb-SiO interface to be significantly higher than that calculated using the measured oxide thickness. Also, a more complete theory of the effect may improve the agreement. It is interesting to note that this modulation of an electron state by an external electric field is a unique example of a quantum-field-effect device.

B. Magnesium

As reported previously,[1] a set of standing-wave states was also observed for Mg films. A typical measurement is shown in Fig. 14 where, over the indicated voltage range, states below the Fermi level in Mg are covered. As for Pb, the splitting is inversely proportional to the thickness. Now, however, the standing-wave states are located below the Fermi level and, based on knowledge of the band structure, a $Q=1$ band-edge commensurate level is involved. As the thickness is changed, the states move with respect to the stationary band-edge state located a little more than 1 eV below the Fermi level.

The amplitude of the effect is generally smaller in Mg than in Pb. The effect never exceeded a 5% change in conductivity, and usually was about 1%. The dependence of amplitude on temperature was less pronounced in the case of Mg and in some films, in fact, there was no change in amplitude between 4 and 77 °K. While no detailed measurements on temperature dependence were made, it does not appear that amplitude temperature dependence is a fundamental, reproducible property for thin-film standing waves. It is similar in a sense to the resistance-ratio measurement on metals, where wide variations can occur and only very perfect metals show large resistance ratios.

It was also reported that a weak, finer structure was usually observed in the opposite polarity in the range 0–1 V. A $Q=2$ state is expected at 1.52 V, but background effects become large above 1.0 V. A $Q=3$ state is expected at about 0.5 V, but usually the $Q=1$ series of resolved states extend through

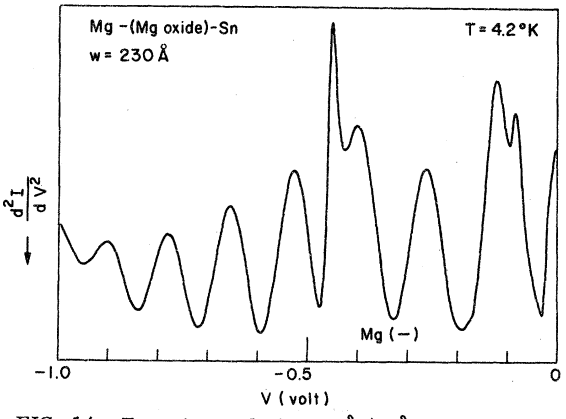

FIG. 14. Experimental plot of d^2I/dV^2 vs V for Mg showing the standing-wave structure associated with an Mg band edge approximately 1.25 eV below the Fermi level. The plot scans energy levels below the Fermi level in Mg. Note the presence of O-H inelastic tunneling peaks at 90 and 450 mV.

0.0 V and into the region of $Q=3$. The structure in this region does not resolve itself into a well-defined series of peaks with one-third the spacing of the $Q=1$ series. The large extent of the $Q=1$ series spans almost one-third of the zone and appears to inhibit the formation of a well defined $Q=3$ series. It would be informative to fabricate Mg film with a lesser smoothness to confine the $Q=1$ series to a smaller energy range. In this case, it is expected that the $Q=3$ series would be resolved.

The data on magnesium can be understood following a procedure similar to that followed for Pb. First, the Mg films are oriented with the [0001] direction perpendicular to the surface of the film. The appropriate section[12] of the band structure is shown in Fig. 15, where the principal set of states of interest derive from the $Q=1$ state. This is band edge located 1.24 eV below the Fermi level. A $Q=2$ state is located 1.52 eV above the Fermi level. The expected intensity distribution of the structure would suggest that the peaks should build up to a maximum at the band edge, contrary to the observation, as is evident in Fig. 14. There the envelope function decreases as the curve approaches -1 V. To understand this behavior, it must be noted in Eq. (14) that there is an exponential term involving both the lifetime of the states as well as v_g, and both of these can contribute to a falloff with energy of the observed peaks. This term evidently dominates the Gaussian term resulting from the size distrubition of the crystal grains. Recall that the energy-vs-momentum curve of Fig. 15 will curve sharply near the band edge and the group velocity will go to zero. However, as is evident from the data, the observed periodicity is too constant with energy to allow for a detailed examination of this curve. As will be seen, the situation is more favorable for Au and Ag. Table II summarizes the band parameters obtained for Mg.

TABLE II. Band parameters for Mg in the [0001] direction compared with the theoretical band structure of Kimball, Stark, and Mullen.

	Theory	Experiment
$E(\pi/d)$ (eV)	-1.24	-1.2 ± 0.1
$v_g(-1$ eV) (cm/sec)	$\sim1.4\times10^8$	1.46×10^8
$E(\frac{1}{2}(\pi/d))$ (eV)	$+1.52$	
$v_g(+1$ eV) (cm/sec)	$\sim1.4\times10^8$	

C. Gold

Gold has an fcc structure and, as for Pb films, has a [111] orientation in textured films. The appropriate band-structure segment is thus the Γ-L branch shown in Fig. 16. There are band edges at about 1 eV below the Fermi level ($L_{2'}$) and 3.6 eV above the Fermi level (L_1). The observation of tunneling structure in thick Au films associated with these edges has been reported by us previously. These $Q=1$ states are good candidates for displaying standing-wave structure. In the case of very thin gold films (90–150 Å), standing-wave structure appears at voltages above 3.6 V and somewhat below -0.9 V. Standing-wave states cannot appear between these voltages because of

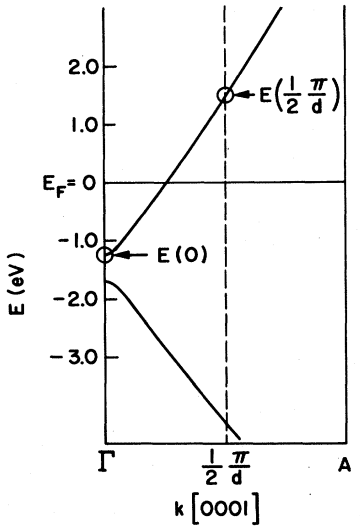

FIG. 15. Plot of a portion of E vs k for Mg (Ref. 12) showing the commensurate states relevant to the present experiment. The energy and group-velocity values are listed in Table I.

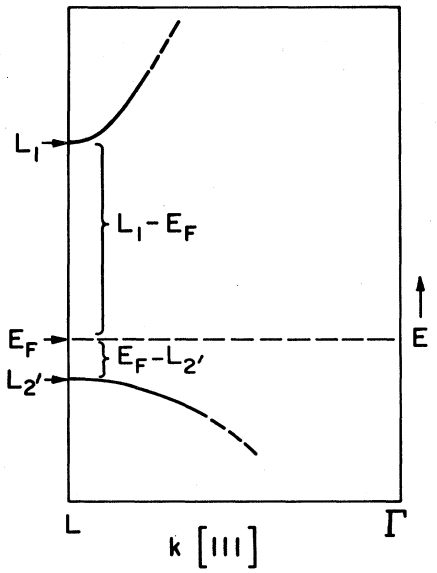

FIG. 16. Sketch of E vs k for Au and Ag showing the [111] direction relevant to the present experiments.

the energy gap in the Γ-L branch.

The tunneling structure at 4.2 °K in the region above 3.6 V is shown in Fig. 17. Because of increasing background, the third derivative of I vs voltage was used to examine better the standing-wave states. Strain modulation at 77 °K was also used to confirm that this structure has the strain sensitivity associated with band states. The upper voltage limit of observation was about 4.4 V, so only a limited segment of this high-energy branch could be studied. The spectrum of Fig. 17 has the following features: There is a peak in the third derivative at 3.65 V which is also present in thick films. This peak is not sensitive to film thickness. At voltages just above this, a set of standing-wave states appear. It is to be noted that the spacing changes with voltage, indicating a curvature in E-k in this region. The zeros in the third derivative locate standing-wave states (recall that peaks in the second derivative locate the energy of standing-wave states when lifetime broadening is considered). An indexing scheme can be derived by noting the shift in these states as the thickness of the film is changed slightly.

A plot can be made of the energy of the states in terms of the allowed values of momentum. This is shown in the upper curve of Fig. 18 where the points indicate the allowed values of $k = n'(\pi/w)$, $n' = 2, 3, \ldots$. The $n' = 1$ state was not distinctly seen, so the sequence begins with the value of $n = 2$. The indexing then permits a direct plotting of the E-k curve near the $Q = 1$ state at the band edge. The curvature corresponds to an effective mass of 0.1 near the band edge.

As with Mg, the envelope of the standing-wave pattern near a band edge will be more complicated than Eq. (14) might indicate, since the tunneling probability is related to the group velocity, which goes to zero at the edge. In addition, the splitting between levels changes significantly as the levels

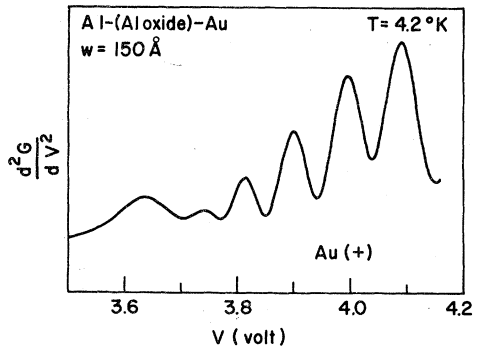

FIG. 17. Experimental plot of d^2G/dV^2 vs V for an Au film indicating the presence of standing-wave states just above the L_1 band edge.

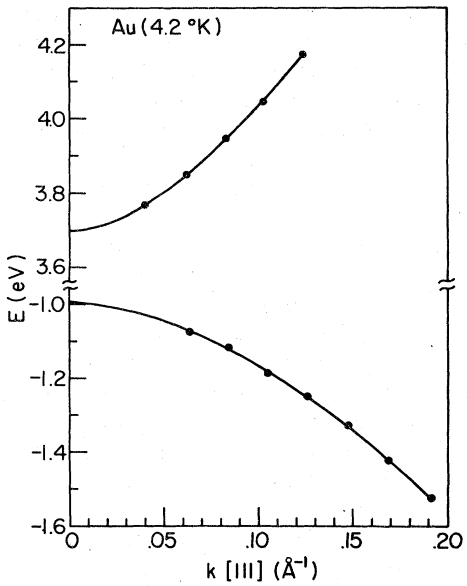

FIG. 18. Experimentally derived plot of E vs k for the $L_{2'}$ and L_1 band-edge states of Au. The points indicate the positions of the observed standing-wave levels for a 150-Å film.

bunch together. This results in a loss of amplitude in the standing-wave pattern. The structure in the third derivative at 3.65 V is slightly below the band edge extrapolated from the curve of Fig. 18. It is clear that "simple" standing-wave theory would not predict such an energy state, since this would correspond approximately to $n' = 0$ and the wave function would not fit the boundary condition of zero amplitude at the surface. It is not surprising, however, that the simple model is not precise in this sense. The energy states in thin films must be examined with a more rigorous approach. Cooper and Bennet[13] have carried out such an analysis for nickel films and they point out that "intrinsic" surface states can occur near bulk band edges. Such states have not been included in our simple model. It is possible that the extra structure appearing in the tunneling spectrum can be attributed to these states. As will be seen, such effects also appear near the $L_{2'}$ point below the Fermi level.

The region below the Fermi level also showed standing-wave structure in the region between 1 and 2 V. The pattern in this case was weaker and showed a very definite change in splitting with voltage, which indicates the curvature of the E-k curve. Again, by plotting allowed k values versus observed energy, the energy band near the $L_{2'}$ point can be plotted. This is the lower curve in Fig. 18, and is best fit with a curve corresponding to an effective mass of 0.25 and by setting the band edge at -1.0 ± 0.1 V.

The energy of the $L_{2'}$ thus determined is some-

what lower than what has been found by less direct methods. In our own earlier work,[6] we assigned the strong structure in the vicinity of −0.6 V to the $L_{2'}$ edge. This structure in the tunneling spectra does not locate the band edge very precisely. It is not clear what this structure represents, but it clearly is associated with the band structure of Au as is indicated by its response to strain. It may be a surface-state effect associated with the Au as mentioned above.

In any case, the standing-wave structure permits the $L_{2'}$ and L_1 points to be located with greater certainty. These values are included in Table III, where our findings are compared with the recent band-theory calculations of Christensen and Seraphin.[14] Our effective-mass values are also shown. While the band theory should also yield a set of effective-mass values, a fairly fine-grained theoretical data tabulation is required. Therefore we were not able to extract accurate effective masses from the calculations, but it is clear that small effective masses of between 0.1 and 0.2 are to be expected.

D. Silver

Silver is very similar to Au in its Γ-L band structure. There should be an $L_{2'}$ edge near the Fermi level and an L_1 edge about 4 eV above the Fermi level. The 4-eV band is outside the range of tunnel junction breakdown for our junctions, so we can only say that the L_1 point is higher than 3.5 eV. The region below the Fermi level revealed a set of standing-wave states associated with the $L_{2'}$ region. The structure was stronger than the corresponding states in Au, but still much weaker than in Pb.

Figure 19 shows a d^2G/dV^2-vs-voltage spectrum between 0.3 and 1.0 V. This corresponds to a set of standing-wave states below the Fermi level of Ag, since the Ag was negative in voltage. There is a strong O-H stretching line at 0.45 V which obscures one of the standing-wave states. The change in spacing between levels is quite evident and the levels tend to bunch together near 0.3 V.

A plot of the E-k curve can be obtained just as for the case of the bands in Au. By using different thicknesses of Ag films a consistent indexing of the n' values with the peaks in the second derivatives can be obtained. This procedure then yields the band edge and the effective mass near the band edge. The resulting section of the E-k curve is shown in Fig. 20. Typical data points are shown for a film 250 Å thick. The "allowed" k values for such a film are multiples of 0.0125 Å^{-1}. The resulting band parameters are included in Table IV and compared with the recent theory of Christensen.[15]

It should be noted that structure was observed just above the $L_{2'}$ edge of Ag at about the Fermi level. This structure was similar to that previously discussed for the case of Au. Again, it appears also for thick films. This structure lies within the L_1-$L_{2'}$ gap and may be ascribed to surface states.

TABLE III. Band parameters for Au in the Γ-L direction compared with the theoretical band structure of Christensen and Seraphin.

	Theory	Experiment
$E(L_1)$ (eV)	+2.99	+3.65±0.05
$E(L_{2'})$ (eV)		0.10
m^* (L_1)	−0.72	−1.0±0.1
m^* $(L_{2'})$		0.25

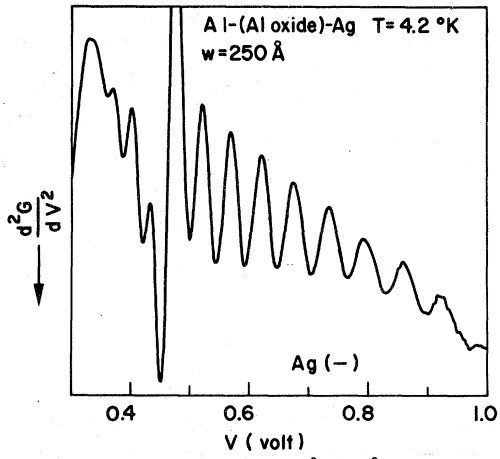

FIG. 19. Experimental plot of d^2G/dV^2 vs voltage for Ag showing the series of standing-wave states just below the $L_{2'}$ edge of Ag, with the edge located at 0.3 eV. Increasing voltage scans energy states in the Ag film below the Fermi level.

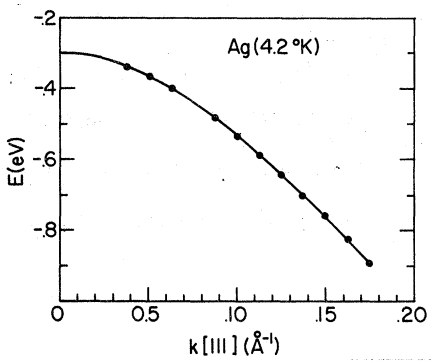

FIG. 20. Plot of experimentally derived E vs k for the [111] direction of Ag. The points indicate a set of data for a film 250 Å thick. This curve locates the $L_{2'}$ point at 0.3 eV below the Fermi level.

TABLE IV. Band parameters for Ag in the Γ-L direction compared with the theoretical band structure of Christensen.

	Theory	Experiment
$E(L_1)$ (eV)	+3.27	>3 (not observed)
$E(L_{2'})$ (eV)	−0.16	−0.3±0.05
$m^*(L_{2'})$		0.17

IV. SUMMARY

The foregoing experiments and discussion have touched upon a number of aspects of standing-wave states in metal films. Electron tunneling has proven to be a tool which clearly reveals the location of such quantum states. It is clear that such experiments lend themselves to a number of other investigations. In addition to the measurement of critical band parameters, the effects associated with the boundaries of the film are of great interest. A coupling of a standing-wave state to a boundary perturbation can reveal details of the added perturbation, e.g., an organic molecule on either surface of the film.

Considering the use of standing-wave states to derive band parameters, the location of the L points in Au and the $L_{2'}$ point in Ag are good examples. Attempts to locate these points using a variety of optical methods[16] has been an effort of long standing. It appears that the method of standing-wave tunneling, when applicable, offers a more certain approach. The major reason is that tunneling spectra reveal directly the positions of band points with respect to the Fermi level. In addition, the directionality of tunneling restricts the measurement to a definite direction in the band structure. Optical transitions, however, locate energies of states with respect to other states, not necessarily with respect to the Fermi level, and also do not usually determine the direction of the portion of the E-k curve involved. These difficulties create serious complications for interpretation not present in tunneling spectroscopy. Possibly, optical samples prepared in a manner which permits standing-wave states to exist could offer a useful clarification of optical experiments.

The other important aspect of standing waves is their potential as a new type of surface probe. It was seen that one could detect an electric field on the side of a thin film remote from the tunnel junction. This detection of surface electric fields could be used to detect chemically produced surface electric fields. This might be particularly interesting in the case of gold films, since the gold surface can be kept free of oxides. The electric fields could then be produced chemically on this free surface and detected by the shift produced on standing-wave states.

ACKNOWLEDGMENTS

The authors wish to thank Dr. L. C. Davis for helpful discussions and R. Ager and E. Schermer for their valuable technical assistance.

[1]R. C. Jaklevic, J. Lambe, M. Mikkor, and W. C. Vassell, Phys. Rev. Lett. 26, 88 (1971); Solid State Commun. 10, 199 (1972).
[2]E. Bauer, in *Single Crystal Films*, edited by M. H. Francombe and H. Sato (Pergamon, New York, 1964), p. 43.
[3]L. C. Davis, R. C. Jaklevic, and John Lambe, Phys. Rev. B 12, 798 (1975).
[4]E. L. Wolf, Phys. Rev. B 10, 784 (1974).
[5]J. J. Quinn, Phys. Rev. 126, 1453 (1962); H. Thomas, Z. Phys. 147, 395 (1957).
[6]R. C. Jaklevic and John Lambe, Surf. Sci. 37, 922 (1973).
[7]L. I. Schiff, *Quantum Mechanics* (McGraw-Hill, New York, 1955), p. 36.
[8]J. Lambe and R. C. Jaklevic, Phys. Rev. 165, 821 (1968).
[9]Model 1070 signal-averaging computer, Nicolet Instrument Corp.
[10]J. R. Anderson and A. V. Gold, Phys. Rev. 139, A1459 (1965).
[11]R. J. Corruccini and J. J. Gniewek, *Thermal Expansion of Technical Solids at Low Temperature*, Natl. Bur. Stand. (U.S.) Monograph 29 (U.S. GPO, Washington, D.C., 1961).
[12]J. C. Kimball, R. W. Stark, and F. M. Mueller, Phys. Rev. 162, 600 (1967).
[13]B. R. Cooper and A. J. Bennett, Phys. Rev. B 12, 4654 (1970).
[14]N. Egede Christensen and B. O. Seraphin, Phys. Rev. B 4, 3321 (1971).
[15]N. Egede Christensen, Phys. Status Solidi B 54, 551 (1972).
[16]R. Rossei, Phys. Rev. B 10, 474 (1974); N. V. Smith, Phys. Rev. B 3, 1862 (1971).